Curved boundaries and chiral instabilities – two sources of twist in homeotropic nematic tori

SCHOLARONE™
Manuscripts

Journal Name

ARTICLE TYPE

Curved boundaries and chiral instabilities – two sources of twist in homeotropic nematic tori

James P. McInerney,[a] Perry W. Ellis,[a,b] D. Zeb Rocklin,[a] Alberto Fernandez-Nieves,[a,c,d] and Elisabetta A. Matsumoto[*a]

Many liquid crystalline systems display spontaneous breaking of achiral symmetry, as achiral molecules aggregate into large chiral domains. In confined cylinders with homeotropic boundary conditions, chromonic liquid crystals – which have a twist elastic modulus which is at least an order of magnitude less than splay and bend counter parts – adopt a twisted escaped radial texture (TER) to minimize their free energy, whilst 5CB – which has all three elastic constants roughly comparable – does not. In a recent series of experiments, we have shown that 5CB confined to tori and bent cylindrical capillaries with homeotropic boundary conditions also adopts a TER structure resulting from the curved nature of the confining boundaries [Ellis *et al., Phys. Rev. Lett.*, 2018, 247803]. We shall call this microscopic twist, as the twisted director organization not only depends on the confinement geometry but also on the values of elastic moduli. Additionally, we demonstrate theoretically the curved geometry of the boundary induces a twist in the escaped radial (ER) texture. Moving the escaped core of the structure towards the center of the torus not only lowers the splay and bend energies, but lowers the energetic cost of this distinct source for twist that we shall call geometric twist. As the torus becomes more curved, the ideal location for the escaped core approaches the inner radius of the torus.

Chirality is ubiquitous in the natural world. A great deal of

chirality observed in biology and chemistry is molecular in origin, yet in soft materials and complex fluids, the achiral can become chiral. This chirality is not microscopic in origin – it is an emergent property arising from interactions between achiral molecules. The spontaneous formation of chiral mesostructures from achiral constituents is a powerful means of generating hierarchical structures[2–8]. Several liquid crystalline systems play host to emergent chirality[3,7,9,10]. Confinement-induced frustration also seeds the formation of chiral domains in liquid crystals[11–14]. In particular, confining chromonic liquid crystals to cylinders with homeotropic (normal) boundary conditions facilitates the formation of chiral domains[15–18]. This is in stark contrast to the classical achiral escape texture predicted for such geometries[19,20]. However, in chromonics, the energetic cost of chiral deformations is at least an order of magnitude lower than other elastic deformations[16,18]. Therefore, such emergent chirality is the lowest energy path to relieving frustration induced by boundary conditions. In a recent series of experiments, Ellis et al.[1] observed chirality in nematic liquid crystals in toroidal droplets with homeotropic boundary conditions. These experiments used 4-cyano-4'-pentylbiphenyl (5CB) which, unlike chromonics, has a cost to twisting that is relatively comparable to that of other elastic deformations $K_2/K_1 \approx K_2/K_3 \approx 0.3$[14]. A simple analysis extending the cylindrical results to tori shows that the achiral configuration should not be stable[21]. Here, we demonstrate that there are two sources for twist in homeotropic tori. In addition to the standard *microscopic twist* – where molecular chirality or elastic constants together with the bounding geometry and director anchoring conditions create a preferential environment for twist – we find that the geometry of the torus (or indeed, a cylinder around any curve of non-zero curvature) itself induces a different type of twist, which we call geometric twist. We show this for the case of escape radial (ER) textures, where the energetic cost associated with *geometric twist*, coming from the doubly curved boundary condition of the torus, is lowered by moving the core off the centerline of the torus.

Nematic liquid crystal phases are formed by anisotropic

[a] *School of Physics, Georgia Institute of Technology, 837 State Street, Atlanta, Georgia, 30332 USA.*

[b] *John A. Paulson School of Engineering and Applied Sciences, Harvard University, 9 Oxford Street, Cambridge, Massachusetts, 02138 USA.*

[c] *Department of Condensed Matter Physics, Universitat de Barcelona, Av Diagonal 647, 08028 Barcelona, Spain.*

[d] *ICREA - Institucío Catalana de Recerca i Estudis Avançats, 08010 Barcelona, Spain.*

∗ Corresponding author: sabetta@gatech.edu
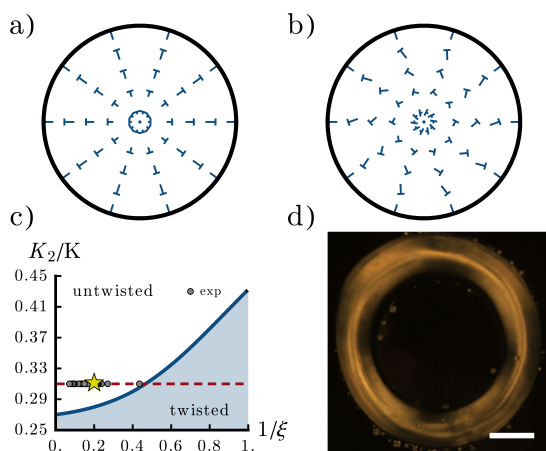
Fig. 1 a) Twistless radial escape of the homeotropic cylinder. b) Twisted radial escape of the homeotropic cylinder. c) A stability analysis for homeotropic tori with centered radial escape. This analysis fails to capture experimental data[1]. The circles correspond to experiments with observed microscopic twist. The star corresponds to the experiment[1] in (d) with $\xi = 5$ which displays microscopic twist. (Image under crossed polarizers. Scale bar = 250 μm.)

molecules which preferentially align with their molecular axes parallel to one another, described by the director field **n**. Low energy elastic deformations from the uniform state are captured by the Frank-Oseen free energy functional[22],

$$F = \frac{1}{2} \int_V dV \left[K_1 (\nabla \cdot \mathbf{n})^2 + K_2 (\mathbf{n} \cdot \nabla \times \mathbf{n})^2 + K_3 (\mathbf{n} \times (\nabla \times \mathbf{n}))^2 \right], \quad (1)$$

where K_1, K_2 and K_3 are the elastic moduli for splay, twist and bend elastic distortions, respectively. In the one-constant approximation $K_1 = K_2 = K_3 = K$, the Frank-Oseen free energy is vastly simplified to $F = \frac{K}{2} \int_V dV |\nabla \mathbf{n}|^2$. However in chromonics, the twist elastic constant is much smaller than the others $K_2 \ll K_1, K_3$, thus deformations that increase the twist free energy are much more favourable than those involving splay or bend.

In a homeotropic cylinder with strong anchoring, an analytic solution for the escaped radial configuration can be calculated by considering a generic nematic director field in cylindrical coordinates of the form $\mathbf{n} = \sin(\Omega(r))\mathbf{e}_r + \cos(\Omega(r))\mathbf{e}_z$, where $\mathbf{e}_z$ points along the axis of the cylinder. In the one-constant approximation, the analytic solution for the escape texture can be found by solving the Euler-Lagrange equation $\ddot{\Omega} + \frac{R}{r}\dot{\Omega} - \frac{R^2}{2r^2}\sin(2\Omega) = 0$ with the boundary conditions $\Omega(r = 0) = 0$ and $\Omega(r = R) = \pi/2$, which yields the solution $\Omega(r) = 2\arctan(r/R)$[16,21,23] depicted in Fig. 1a.

Microscopic twist can be introduced to the homeotropic cylinder by including the scalar field $\Lambda(r)$ in the director $\mathbf{n} = \sin(\Omega(r))\cos(\Lambda(r))\mathbf{e}_r + \sin(\Omega(r))\sin(\Lambda(r))\mathbf{e}_\theta + \cos(\Omega(r))\mathbf{e}_z$[16]. After relieving the one-constant approximation, in particular choosing $K_2 < K = K_1 = K_3$, the corresponding Euler-Lagrange equations still admit stationary solutions which are microscopically twistless $\Lambda = 0$. Examining the second order condition for stability

$$\delta^2 F = \sum \frac{\delta^2 F}{\delta u_i \delta u_j} \delta u_i \delta u_j > 0, \quad (2)$$

for $\{u_i = \Lambda, \partial_\rho \Lambda, \partial_\psi \Lambda\}$, shows that if $K_2 \lesssim 0.27K$ such microscopically twistless solutions are unstable to perturbations in Λ, as depicted in Fig. 1b. Note that the free energy is already minimized in respect to Ω and allowing for perturbations $\delta\Omega$ does not affect the above result.

Theories for spontaneous breaking of achiral symmetry in liquid crystal-filled solid tori used angular toroidal coordinates[21,24]. In these coordinates, the escaped core lives at the center of the circular cross-section of the torus. When solving the Euler-Lagrange equations for the minimal energy director field, the singularity in the coordinate system becomes the line along which escape occurs. A stability analysis of the centered escape (see 1c, ESI) shows the maximal K_2/K ratio that admits stable microscopically twisted configurations. As with homeotropic cylinders, microscopically twistless ($\Lambda = 0$), angularly symmetric ($\Omega(r, \theta, z) = \beta(r)$) solutions in homeotropic tori are unstable below a critical twist modulus – they adopt configurations with microscopic twist ($\Lambda \neq 0$). This critical modulus increases with the curvature of the torus, as shown in Fig. 1c. However, experiments with toroidal droplets made from 5CB, where $K_2/K \approx 0.31$, yield polarized images (eg. Fig. 1d) which reveal features indicative of microscopic twisting well into the predicted stable twistless regime[1].

The assumption, adopted from cylindrical confinement, that the escape core lives in the center of the circular cross section is implicitly broken when the cylinder becomes curved around the $\mathbf{e}_z$-axis. As the aspect ratio of the torus $\xi = R_o/R_i$, where R_o is the radius from the origin to the center of the tube of the torus and R_i is the radius of the tube, decreases, splay from the boundary condition near the center of the torus increases from $(\nabla \cdot \mathbf{n})^2 \to 0$ as $\xi \to \infty$ to $(\nabla \cdot \mathbf{n})^2 \to \infty$ as $\xi \to 1$. One route to decrease the splay for tori with low ξ is to shift the location of the escape core.

In order to accommodate this necessary shift in the escape core, we consider a set of coordinates that maintains homeotropic boundary conditions along the outside of the torus, but allows the central escape to exist anywhere within the solid torus. To do this, we choose a conformal coordinate change using Möbius transformations, which are given by the map $w \to \frac{aw+b}{cw+d}$, $w \in \mathbb{C}$, $a, b, c, d \in \mathbb{R}$. Three points define a Möbius transformation. We want a transformation that leaves the boundary of the unit disk unchanged, but moves the center of the coordinate system from the origin to an arbitrary point inside the unit disk $\sigma \in \mathbb{C}$. Our Möbius transformation,

$$w \to \frac{-w + \sigma}{-\bar{\sigma}w + 1}, \quad (3)$$

takes the coordinate singularity at the origin of polar coordinates and maps it to a point $\{\text{Re}(\sigma), \text{Im}(\sigma)\}$ (see Fig. 2b). However, there is nothing to break the top-bottom symmetry of the torus, so we can choose a shift that is purely real, corresponding to $\text{Im}(\sigma) = 0$. By rewriting the imaginary coordinate $w = \rho e^{i\psi}$ (see Fig. 2c), we arrive at a distorted set of polar coordinates, where we can easily write the homeotropic boundary condition at $\rho = 1$ and the escape boundary condition at $\rho = 0$. To create the offset toroidal coordinates, shown in Fig. 2d, the unit disk in the xz-plane is translated by the aspect ratio of the torus ξ in the $\mathbf{e}_x$ direction and revolved around the z-axis,
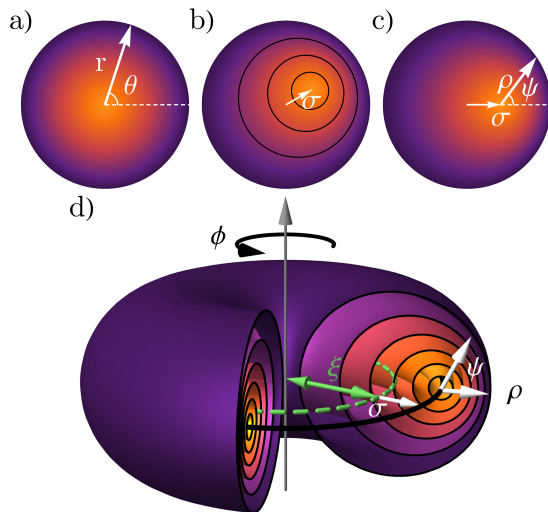
Fig. 2 The conformal transformation $w \to \frac{-w+\sigma}{-\bar{\sigma}w+1}$ moves the core of an escaped radial texture from the origin (a) to the point $\{\mathrm{Re}(\sigma), \mathrm{Im}(\sigma)\}$ (b). c) In the resulting coordinate system, ρ and ψ are the transformed radial and azimuthal coordinates, with origin at $(\sigma, 0)$. d) To create a set of toroidal coordinates, the origin is offset by ξ and revolved around the z-axis. (Note that in this figure, we show $\sigma > 0$. Our minimization finds $\sigma < 0$ in all cases.)

$$x = \left(\frac{\rho(\sigma^2+1)\cos(\psi) - (\rho^2+1)\sigma}{\rho^2\sigma^2 - 2\rho\sigma\cos(\psi)+1} + \xi \right) \cos(\phi),$$

$$y = \left(\frac{\rho(\sigma^2+1)\cos(\psi) - (\rho^2+1)\sigma}{\rho^2\sigma^2 - 2\rho\sigma\cos(\psi)+1} + \xi \right) \sin(\phi),$$

$$z = \frac{\rho(\sigma^2-1)\sin(\psi)}{-\rho^2\sigma^2 + 2\rho\sigma\cos(\psi)-1}. \tag{4}$$

In these coordinates, a generic director field has the form

$$\mathbf{n} = \cos(\alpha)\sin(\beta)\mathbf{e}_\rho + \sin(\alpha)\sin(\beta)\mathbf{e}_\psi + \cos(\beta(\rho))\mathbf{e}_\phi, \tag{5}$$

where β is the escape angle, α describes the microscopic twist, and we are restricted to the angularly symmetric case in which the director field has no ψ dependence. The homeotropic boundary conditions and radial escape are satisfied by

$$\alpha|_{\rho=1} = 0, \quad \partial_\rho \alpha|_{\rho=0} = 0, \quad \beta|_{\rho=1} = \frac{\pi}{2}, \quad \beta|_{\rho=0} = 0, \tag{6}$$

where the second condition on α is necessary to ensure the existence of stationary solutions for the free energy[21]. The metric tensor associated with the coordinates in Eqn. 4 is computed $g_{ij} = \partial_i \mathbf{r} \cdot \partial_j \mathbf{r}$, $i, j \in \{\rho, \psi, \phi\}$, yielding non-zero components

$$g_{\rho\rho} = \frac{(\sigma^2-1)^2}{\left(\rho^2\sigma^2 - 2\rho\sigma\cos(\psi)+1\right)^2}, \quad g_{\psi\psi} = \frac{\rho^2(\sigma^2-1)^2}{\left(\rho^2\sigma^2 - 2\rho\sigma\cos(\psi)+1\right)^2}, \tag{7}$$

$$g_{\phi\phi} = \frac{\left(\xi\rho^2\sigma^2 - \rho(2\xi\sigma + \sigma^2 + 1)\cos(\psi) + \xi + \rho^2\sigma + \sigma\right)^2}{\left(\rho^2\sigma^2 - 2\rho\sigma\cos(\psi)+1\right)^2}.$$
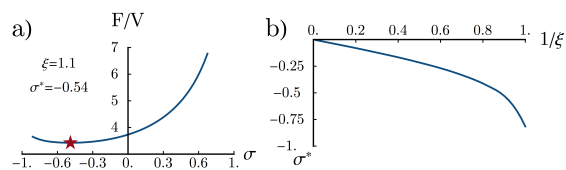
Fig. 3 a) Normalized Frank-Oseen free energy for $\alpha = 0$, $\beta = \beta(\rho)$ satisfying the associated Euler-Lagrange equations with aspect ratio $\xi = 1.1$ as a function of σ. This gives a minimal value at $\sigma^* = -0.54$. b) Dependence of σ^* on aspect ratio where $1/\xi = 0$ corresponds to cylinders and $1/\xi \to 1$ is the limit of the horn torus.

In curvilinear coordinates, the vector derivatives are given by

$$\nabla \cdot \mathbf{b} = \frac{1}{\sqrt{g}} \partial_i \left(\frac{\sqrt{g} b_i}{h_i} \right), \quad \nabla \times \mathbf{b} = \mathbf{e}_i \frac{1}{\sqrt{g}} \varepsilon_{ijk} \partial_j (h_k b_k), \tag{8}$$

where $h_i = \sqrt{g_{ii}}$ are the Lamé coefficients, g is the determinant of the metric tensor and ε_{ijk} is the Levi-Civita tensor.

We solve the Euler-Lagrange equations associated with the Frank-Oseen free energy in the one-constant approximation for a director field given by Eqn. 5 with $\alpha = 0$, $\beta = \beta(\rho)$ satisfying the boundary conditions of Eqn. 6 over the domain of escape shifts $-1 < \sigma < 1$ and aspect ratios $0 \le \frac{1}{\xi} < 1$. This is an *ansatz* for a microscopically twistless solution, i.e. an ER texture. The extremal values of $\frac{1}{\xi}$ correspond to a cylinder for $\frac{1}{\xi} \to 0$ and the horn torus (a torus with no "hole" in the middle) as $\frac{1}{\xi} \to 1$. Even the (microscopically twistless) centered radial escape solution, $\sigma = 0$, has non-zero twist energy,

$$F_t = \int_0^1 d\rho \frac{\pi\rho \sin^2(2\beta(\rho))}{2\left(\sqrt{\xi^2 - \rho^2} + \xi\right)}, \tag{9}$$

corresponding to twisting within planes of constant z, independent of the elastic moduli. This geometric twisting vanishes as $\frac{1}{\xi}$ when approaching the homeotropic cylinder.

We find the ideal escape shift σ^*, the value of σ that minimizes the free energy, for each value of ξ, as shown in Fig. 3a for $\xi = 1.1$. We see in Fig. 3b that all tori admit a shifted radial escape in the one-constant approximation. While the particular elastic moduli affect the exact magnitude of this escape shift, an inward shift $\sigma < 0$ reduces the free energy (see ESI). In such geometries, the director field must twist in order to satisfy the boundary conditions. An example director field for the $\xi = 1.1$ torus is shown in Fig. 4a. The leading order addition to the twist energy Eqn. 9

$$\delta F_t = \int_0^1 d\rho \, \pi\rho \sin^2(2\beta(\rho))\sigma \tag{10}$$

is negative for all tori, since all σ^* are negative. Hence, there is geometrically induced twist in both the $z = $ constant and $\phi = $ constant planes, where the latter reduces the overall twist energy. By comparing the free energy of the shifted escape texture with the centered escape, we find the geometrically induced twist decreases all three components of the free energy (see Fig. 4b-f). There is a slight increase in the free energy near the inner radius of the torus due to splay and bend. However, this is more than compensated for by
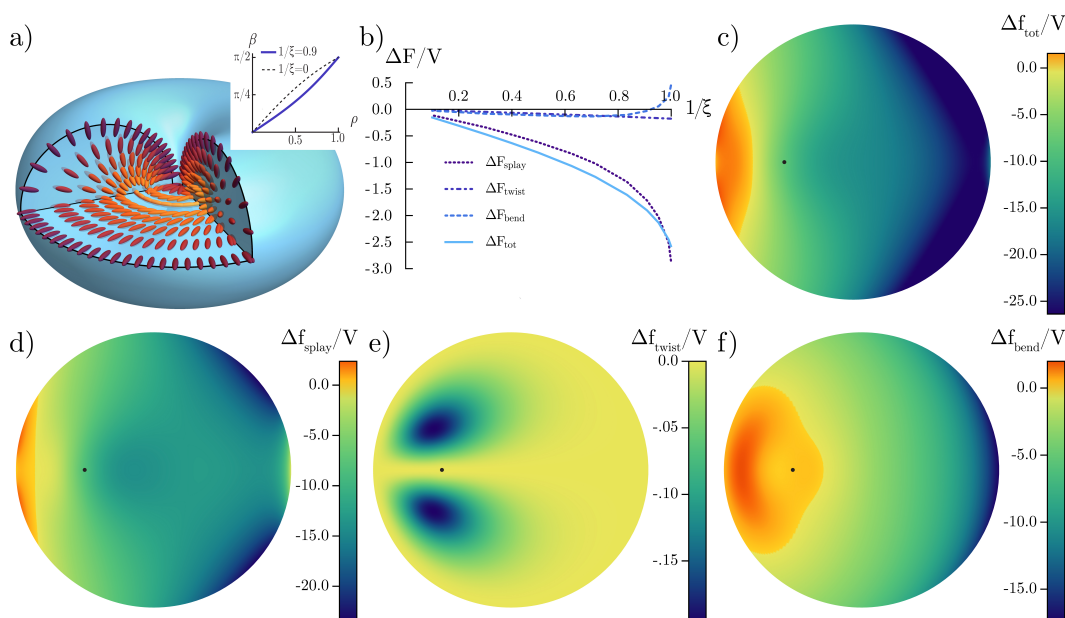
Fig. 4 a) The minimal energy radial escape director field with $\alpha = 0$ (twistless) and $\beta(\rho)$ plotted in the inset for $\xi = 1.1$, $\sigma = -0.54$. b) The total changes in energy after integrating over the cross section of the torus, $\Delta F/V = \int_V (f(\sigma = \sigma^*) - f(\sigma = 0))/V$ for splay, twist, bend and the one constant approximation all decrease as $1/\xi$, except for bend, which increases near the horn torus limit. c) The total change in energy density in the one-constant approximation $\Delta f/V = (f(\sigma = \sigma^*) - f(\sigma = 0))/V$ for the energy minimizing director field and shifted escape core compared with the centered core decreases away from the center of the torus. From the component energy densities, (d-f) the splay (d) and bend (f) energies are slightly increased near the inner radius of the torus, but decrease significantly towards the outer radius of the torus. However, the twist (e) decreases as the escaped core shifts inwards.

the decrease in free energy density towards the outer radius of the torus. Near the limit of the horn torus, shifting the escape increases the total cost to bend distortions, however the total energy is still reduced by the contributions of the splay and twist energies.

A small twist elastic constant compared with splay and bend elastic constants is frequently responsible for the spontaneous breaking of achiral symmetry in confined nematics with frustrated boundary conditions. We have demonstrated that, in homeotropic tori, it is energetically favourable from the point of view of all three elastic deformations, to have also an induced geometric twist associated with shifting the escaped centerline. Although the additional microscopic twist associated to the TER texture is present in the experiments[1], the ubiquitous geometric twist causing the shift of the escape core towards the inside of the torus, might also be playing a role. Determining this contribution requires relieving our symmetry assumptions on the director field before minimizing the free energy over all values of the escape shift. The stability line in Fig. 1c is then given by the ratio K_2/K, if any, for which such solutions are microscopically twisted. Our work opens the door to these additional studies by demonstrating the importance of geometric twist in homeotropic nematic tori with a ER texture. In conjunction with recent work with planar anchoring[23,24], a doubly-curved confinement geometry appears to provide twisting mechanisms regardless of boundary conditions.

Conflicts of interest

There are no conflicts to declare

Notes and references

1 P. W. Ellis, K. Nayani, J. P. McInerney, D. Z. Rocklin, J. O. Park, M. Srinivasarao, E. A. Matsumoto and A. Fernandez-Nieves, *Phys. Rev. Lett.*, 2018, **121**, 247803.
2 G. Pickett, M. Gross and H. Okuyama, *Phys. Rev. Lett.*, 2000, **85**, 3652.
3 D. Walba, *Materials-Chirality*, John Wiley and Sons, 2003, pp. 457–518.
4 M. Ávalos, R. Babiano, P. Cintas, J. Jiménez and J. Palacios, *Tetrahedron: Asymmetry*, 2004, **15**, 3171–3175.
5 L. Tortora and O. Lavrentovich, *Proc. Nat. Acad. Sci.t*, 2011, **108**, 5163–5168.
6 H.-Y. Lee, H. Oh, J.-H. Lee and S. R. Raghavan, *J. Am. Chem. Soc.*, 2012, **134**, 14375–14384.
7 A. Dastan, W. J. Frith and D. J. Cleaver, *J. Phys. Chem.*, 2017, **121**, 9920–9928.
8 A. Dastan, E. A. Matsumoto, W. J. Frith and D. J. Cleaver, *Mol. Phys.*, 2018, **116**, 2823–2835.
9 L. E. Hough, M. Spannuth, M. Nakata, D. A. Coleman, C. D. Jones, G. Dantlgraber, C. Tschierske, J. Watanabe, E. Korblova, D. M. Walba, J. E. Maclennan, M. A. Glaser and N. A. Clark, *Science*, 2009, **325**, 452–456.
10 L. E. Hough, H.-T. Jung, D. Krüerke, M. S. Heberling, M. Nakata, C. Jones, D. Chen, D. R. Link, J. Zasadzinski, G. Heppke, J. P. Rabe, W. Stocker, E. Körblova, D. M. Walba, M. A. Glaser and N. A. Clark, *Science*, 2009, **325**, 456–460.
11 H.-S. Kitzerow, B. Liu, F. Xu and P. P. Crooker, *Phys. Rev. E*, 1996, **54**, 568–575.
12 M. Ambrozic and S. Zumer, *Phys. Rev. E*, 1996, **54**, 5187–5197.
13 J. Jeong, Z. Davidson, P. Collings, T. Lubensky and A. Yodh, *Proc. Nat. Acad. Sci.*, 2014, **111**, 1742–1747.
14 S. Całus, M. Busch, A. V. Kityk, W. Piecek and P. Huber, *J. Phys. Chem. C*, 2016, **120**, 11727–11738.
15 E. Pairam, J. Vallamkondu, V. Koning, B. C. van Zuiden, P. W. Ellis, M. A. Bates, V. Vitelli and A. Fernandez-Nieves, *Proc. Nat. Acad. Sci.*, 2013, **110**, 9295–9300.
16 J. Jeong, L. Kang, Z. Davidson, P. Collings, T. Lubensky and A. Yodh, *Proc. Nat. Acad. Sci.*, 2015, **112**, E1837–E1844.
17 Z. Davidson, L. Kang, J. Jeong, T. Still, P. Collings, T. Lubensky and A. Yodh, *Phys. Rev. E*, 2015, **91**, 050501.
18 K. Nayani, R. Chang, J. Fu, P. W. Ellis, A. Fernandez-Nieves, J. O. Park and M. Srinivasarao, *Nat. Comm.*, 2015, **6**, 8067.
19 P. E. Cladis and M. Kléman, *J. Phys.*, 1972, **33**, 591–598.
20 R. B. Meyer, *Phil. Mag.*, 1972, **27**, 405–424.
21 F. Milan, *MSc thesis*, Leiden University, 2015.
22 F. C. Frank, *Discussions of the Faraday Society*, 1958, **25**, 19–28.
23 T. C. Lubensky, *Mol. Cryst. Liq. Cryst.*, 2017, **646**, 235–241.
24 V. Koning, B. C. van Zuiden, R. D. Kamien and V. Vitelli, *Soft Matter*, 2014, **10**, 4192–4198.